

TinySense: A Lighter Weight and More Power-efficient Avionics System for Flying Insect-scale Robots.

Zhitao Yu^{*,1,3}, Joshua Tran^{*,2}, Claire Li², Aaron Weber¹, Yash P.Talwekar¹, Sawyer Fuller^{1,2}

Abstract—In this paper, we investigate the prospects and challenges of sensor suites in achieving autonomous control for flying insect robots (FIRs) weighing less than a gram. FIRs, owing to their minuscule weight and size, offer unparalleled advantages in terms of material cost and scalability. However, their size introduces considerable control challenges, notably high-speed dynamics, restricted power, and limited payload capacity. While there have been notable advancements in developing lightweight sensors, often drawing inspiration from biological systems, no sub-gram aircraft has been able to attain sustained hover without relying on feedback from external sensing such as a motion capture system. The lightest vehicle capable of sustained hover—the first level of “sensor autonomy”—is the much larger 28 g Crazyflie. Previous work reported a reduction in size of that vehicle’s avionics suite to 187 mg and 21 mW. Here, we report a further reduction in mass and power to only 78.4 mg and 15 mW. We replaced the laser rangefinder with a lighter and more efficient pressure sensor, and built a smaller optic flow sensor around a global-shutter imaging chip. A Kalman Filter (KF) fuses these measurements to estimate the state variables that are needed to control hover: pitch angle, translational velocity, and altitude. Our system achieved performance comparable to that of the Crazyflie’s estimator while in flight, with root mean squared errors of 1.573 degrees, 0.186 m/s, and 0.139 m, respectively, relative to motion capture.

I. INTRODUCTION

Insect-scale robots have the potential to be deployed in the thousands or millions to perform “fast, cheap, and out of control” space missions, collective assembly tasks, or hazard detection, owing to their small size and low materials cost. Recent incarnations of sub-gram aircraft have demonstrated controlled flight [1], [2], as well as electromagnetically-mediated power delivery [3], [4], [5]. But sensor autonomy, that is, the ability to hover without external feedback, has not yet been demonstrated below 10 g, never mind 1 g. A central question is “What are the minimum sensor suite and computation resources needed for the task of flight control?” Of particular concern when designing such a control architecture is how the physics of scale affects sensing and control. The paper [6] serves as a step toward a missing but complementary analysis to previous work that has largely focused on scaling effects on actuation and mechanics in small robots [7], [8], [9], [10].

This research was partially supported by the National Science Foundation through awards ECCS-2054850 and CNS-2235207

* Authors contributed equally.

¹Department of Mechanical Engineering, University of Washington, Seattle, WA, USA

²Paul G. Allen School of Computer Science, University of Washington, Seattle, WA, USA

³Department of Applied Mathematics, University of Washington, Seattle, WA, USA

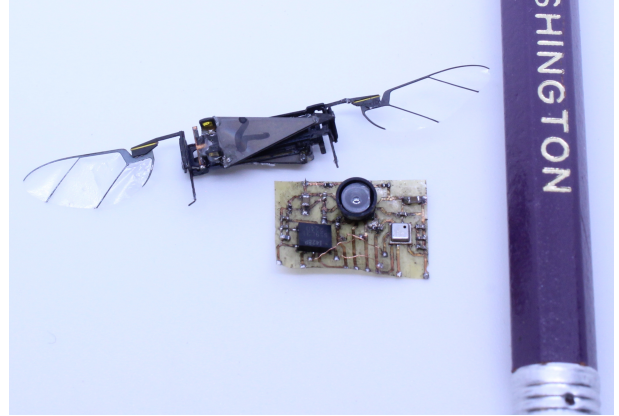


Fig. 1: The TinySense sensor suite shown next to a U. Washington Robofly and a standard pencil for scale. The width of the sensor suite board is approximately 12 mm and its mass is 78.4 mg.

Insect-scale robots have extreme size, speed, weight, and power (SSWaP) constraints. “Sensor autonomy” including stable hovering, represents first level of autonomy in the hierarchy proposed in [11], and is the foundation upon which higher level capability is built. We impose a requirement that sensing and computation to take no more than 10% of the power required to stay in the air; any more than this and flight time is severely impacted. This factor holds for important examples of autonomous drones, such as the 1.5 kg system in [12] and the 30 g system in [13]. This suggests a power budget of ~ 20 mW for a 150 mg Robofly (Figure 1) that consumes 100 mW to fly (about 200 mW after losses from a 50% efficient boost converter are factored in).

The sensing system is very crucial for robots. Large drones can have more payloads to hold sensors onboard such as inertial measurement units (IMUs) and the global positioning system (GPS). However, GPS does not work well in indoor environments [14] and small robots are not able to hold many sensors due to constraints in size, speed, weight, and power consumption (SSWaP). There are several work done on the sensor suite for insect-scale robots [15], [6], [16]. The most recent sensor suite is 187 mg and consumes 21 mW [15].

In this manuscript, we introduce a new avionics system for autonomous hovering flight that is even better tailored in mass and energy consumption for an insect-scale robot (Fig. 3) than previous work [15]. To do so, we made two key refinements to lower power and mass. First, we replaced the power-hungry laser rangefinder with a pressure sensor.

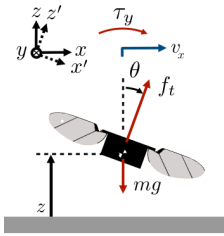


Fig. 2: Forces and state variables of a small hovering Flying Insect Robot (FIR).

In recent years these have attained sufficient precision to be used for the purpose of altitude estimation and control even for insect-scale robots. Second, we replaced the optic flow sensor with a global shutter camera and compute optic flow on a microcontroller, resulting in a reduction in weight from 97 mg to 44 mg. As in [15], this new sensor suite is able to estimate the crucial variables that are needed for controlled flight: pitch angle, translational velocity, and altitude.

Our contributions, in order of importance, are:

- 1) A significant reduction in weight of the sensor suite to 78.4 mg which is less than half of the previous lightest sensor suite [15].
- 2) We showed that we were able to make accurate estimates of the state variables pitch angle, translational velocity, and altitude using data collected wirelessly from this sensor suite while it was mounted on a flying helicopter.
- 3) Implemented an optic flow algorithm on a microcontroller.

Subsequent sections elucidate the dynamics, sensor configurations and measurement models, and corroborate our findings with data acquired wirelessly from our sensor suite, which is then analyzed on a desktop computer.

II. METHODOLOGY

A. Dynamics

The basic dynamics of most small hovering devices are unstable in pitch angle and position. This was true for the first robotic flies [17] and EHD thruster actuated robots [18], as well as larger aircraft such as the tailless Delfly Nimble [19]. Techniques to stabilize them passively through modification of wing configuration [20] or using air dampers [21] are either unproven or result in undesirable steady-state oscillations, respectively. To stabilize these dynamics, we will use a linearized dynamical model from which we will construct an observer of these unstable states so that they can be controlled.

Figure 2 depicts forces acting on a flapping-wing robot such as a gnat robot or the Robofly, but the proposed model can apply to almost any small flying aircraft, including EHD-based thrusters [22].

Near hover, the vehicle’s dynamics are well approximated by a linear state-space model [23], [24], [21] of the form $\dot{\mathbf{q}} = \mathbf{A}\mathbf{q} + \mathbf{B}\mathbf{u} + \mathbf{G}\mathbf{w}$, where \mathbf{w} is the process noise, assumed to be roughly zero-mean Gaussian white noise with known

covariance. Process noise \mathbf{w} is included because it is a necessary consideration for the design of the estimator.

To simplify the analysis, we restrict our attention to motion in the x - z plane; the dynamics in the y - z plane are very similar. We choose a minimal state vector $\mathbf{q} = [\theta, v_x, z]^T$, where θ is the pitch angle, v_x is the vehicle’s translational velocity in the world x -direction, and z is its vertical position or altitude (Fig. 2). When the nonlinear Euler-Lagrange equation dynamics are linearized by taking the Jacobian at $\theta = 0$, thrust force $f_t = mg$, and $z = z_d$, where z_d is the desired altitude, the dynamics matrices are given by:

$$\mathbf{A} = \begin{bmatrix} 0 & 0 & 0 \\ g & -\frac{b}{m} & 0 \\ 0 & 0 & 0 \end{bmatrix}, \quad \mathbf{B} = \begin{bmatrix} 1 \\ 0 \\ 0 \end{bmatrix} \quad (1)$$

, where m is the vehicle’s mass, and b is the vehicles translational drag proportionality constant [16]. Note that because we are concerned in this paper about only estimation, we ignore inputs from the motor, and instead use the measurements of the gyroscope $\mathbf{u} = [\omega_m]$ as the only input. This is discussed further in Section V.

III. SENSOR SUITE AND MEASUREMENTS

Next we consider the sensor suite and state estimator. Our interest is in sensors that are either available commercially off-the-shelf, nearly so, or can be fabricated using the same tools that have been successful building insect robots such as the Robofly [25] and Robobee [26], [1]. A further constraint is that they require extremely low power for both the sensor itself and subsequent transduction and processing. This largely eliminates sensors that emit power, such as radar, sonar, depth cameras that emit structured light, and scanning laser rangefinders [27], but permits passive sensing such as vision. The global positioning system is largely denied indoors and does not provide enough resolution anyway (1–10 m), and, further, requires significant power for signal processing. A lightweight and low-power sensing modality that can provide the necessary information to hover is “optic flow,” which is defined as the velocity of the image (in rad/s) across the camera imager [28]. In tandem with other sensors, optic flow can be used to estimate the distance to obstacles as the imager translates through space [29]. Methods for estimating optic flow include calculating luminance gradients locally [30] (Lucas-Kanade), or image-wide [31], as well as iterative search for matching blocks of pixels [32]. Distances can also be estimated with a second camera and stereo vision using line matching [33], but this requires a second camera and a long “baseline” between cameras for accuracy, which would add too much weight.

Given these constraints, we propose the following set of onboard sensors: An optical sensor, a pressure sensor, and a gyroscope. We designed a customized microcircuit with the three sensors. (Fig. 3)

A. The camera and optic flow

The system employs an optical sensor, the PAG7920LT (PixArt Imaging, Inc., Taiwan), to capture 160×120 QQVGA images at 100 Hz over a 32 MHz SPI connection, with

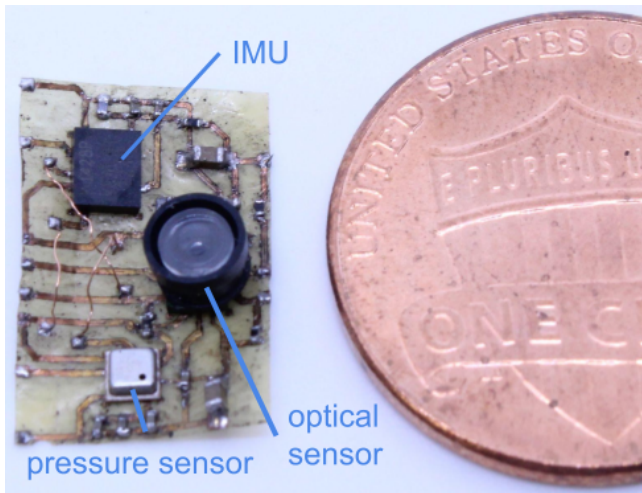


Fig. 3: (a) Sensor suite (PAG7920LT optical sensor, ICM42688-P IMU, BMP388 pressure sensor) next to penny.

which the microcontroller computes optic flow via the Lucas-Kanade Method. The reason we select this camera is that, to our knowledge, it is the only global shutter camera that provides an SPI interface to transmit the image data. Other global shutter cameras require a special interface called MIPI (mobile industry processor interface), which is not available for any microcontroller. The majority of cameras employ a “rolling shutter” in which pixel rows are captured at sequential periods of time. A global shutter camera, by contrast, captures that all pixels at the same time, which ensures an accurate optic flow measurement.

To minimize the data transmitted wirelessly over Bluetooth from our TinySense sensor suite, it is necessary to perform all optic flow calculations onboard. We wrote a Lucas-Kanade algorithm using the Arduino development environment in C++ to run on NRF52-based Adafruit Express board, chosen for its low size and weight.

The Lucas-Kanade algorithm is performed by calculating the following quantities:

$$A = \begin{bmatrix} I_x(q_1) & I_y(q_1) \\ I_x(q_2) & I_y(q_2) \\ \dots & \dots \\ I_x(q_n) & I_y(q_n) \end{bmatrix} \mathbf{v} = \begin{bmatrix} V_x \\ V_y \end{bmatrix} \mathbf{b} = \begin{bmatrix} -I_t(q_1) \\ -I_t(q_2) \\ \dots \\ -I_t(q_n) \end{bmatrix}$$

, where q_1, q_2, \dots, q_n are the brightness readings of each of the n pixels in the image, \mathbf{v} is the image flow in pixels per frame, and $I_x(q_i), I_y(q_i), I_t(q_i)$ are the image’s horizontal, vertical, and temporal (time) partial derivatives respectively, at pixel q_i . Then, the optic flow is estimated (in pixels/frame) by taking the pseudoinverse $\mathbf{v} = (A^T A)^{-1} A^T \mathbf{b}$.

To minimize computation for the limited microcontroller resources, we reduced the image resolution by a factor of 4 (producing a 40×30 resolution) by skipping pixels.

The two most expensive operations involve computing $A^T A$ and $A^T \mathbf{b}$. A 40×30 image produces an A matrix with $(40 - 2) * (30 - 2) = 1064$ rows and 2 columns and a \mathbf{b} matrix with 1064 rows and 1 column. We estimate

multiplying two matrices of size $k \times l$ and $l \times m$ will require kml multiplications. Thus, computing $A^T A$ and $A^T \mathbf{b}$ require 4256 and 2128 multiplications, respectively. We neglect the additional operations required to compute their product (2 multiplications) and the 2×2 matrix inverse (6 multiplications and one divide), giving a total operations count of 6384.

We additionally implemented a form of sparse optic flow in which flow vectors were computed for twelve 10×10 patches, which are averaged to produce a final estimate. A 10×10 image produces an A matrix with $(10 - 2) * (10 - 2) = 64$ rows and 2 columns and a \mathbf{b} matrix with 64 rows and 1 column. Thus, computing $A^T A$ and $A^T \mathbf{b}$ require approximately 256 and 128 multiplications, respectively. With twelve matrices of size 10×10 , the total number of multiplication is $12(256 + 128) = 4608$. This is a reduction of approximately 39%. In the future, we will evaluate these patches individually to remove outliers, removing patches with low eigenvalues (low contrast) or significantly different eigenvalues (aperture problem).

To convert the image flow in pixels/frame to angular velocity in radians/s, we rotated the TinySense by hand and minimized the error between the optic flow measurement multiplied by a constant α and the gyroscope reading. This constant, which depends on the pixel density and field of view of the camera, is given by $\alpha = -0.027$ rad/pixel.

B. Pressure sensor

Altitude measurements are conducted by a Bosch BMP388 pressure sensor. This sensor estimates altitude as a proportion of the difference between the surrounding air pressure and sea level. We set it for $2 \times$ pressure oversampling and an IIR filter coefficient of 3 to maximize resolution. To compensate for variations in local pressure causing inaccurate altitude measurements, the sensor was assigned a bias equal to the average of the first 25 measurements where the sensor system was grounded; this bias was subtracted from every reading.

C. The gyroscope

For the onboard inertial measurement unit (IMU), we chose the TDK ICM42688-P because it is a recent model that is available in the smallest commercially-available package size of 2.5×3 mm. It includes both a 3-axis gyroscope and a 3-axis accelerometer. In this work, we used only the gyroscope, which measures angular velocity through the detection of Coriolis forces within an electromechanical resonator. We configured the sensor to have a ± 2000 degrees/s full-scale (FS) range and enabled the sensor-provided low-noise mode to improve the sensitivity and minimize noise. During initial experiments, we noticed that the gyroscope’s signal was noisier than expected and differed significantly from the Crazyflie’s gyroscope, even after applying a digital low-pass filter. In handheld, non-flying experiments, however, the gyroscope proved accurate. We hypothesized that vibrations from the spinning propellers, which were at a higher frequency than the 100 Hz sampling rate, were introducing aliasing. We enabled the sensor’s anti-aliasing low-pass filter

TABLE I: Comparison between TinySense and prior work

	component	size (mm)	mass (mg)	power (mW)
prior work [15]	IMU	2.5×3×0.91	14	3
	rangefinder	4.9×2.5×1.56	16	5
	optical flow	5×5×3.08	97	12
	board/discretes	–	60	–
	total	–	187	21
TinySense	IMU	2.5×3×0.91	14	3
	pressure	2.0×2.0×0.75	14	2.6
	camera chip	2.2×2.7×6.9	24	10
	lens	3.8×3.8×1.95	20	–
	board/discretes	–	26.4	–
	total	–	78.4	15.6

with a cutoff frequency of 42 Hz, which is well below the Nyquist frequency associated with the 100 Hz sampling rate. We found that this setting significantly reduced the gyroscope’s noise and error.

IV. STATE ESTIMATION

To implement a Kalman Filter, we must first ascertain whether our system is observable at equilibrium. To show this, we linearize the observation model for the task of hovering. Note that the gyroscope provides a low-noise measurement of angular velocity ω . In cases like this, where the sensor provides more precise information than can be derived from knowing the system’s actuated inputs (e.g. the torque applied by the aircraft’s rotors or wings), it is common practice to re-formulate the Kalman Filter to use the sensor’s readings as its "input" u , rather than the actual system input. Doing this has the additional advantage that for each such measurement, one less state variable is required, reducing computation requirements and complexity. In this case, it means that the angular velocity ω need not appear among the state variables. The following is our observation model for the suite of sensors, which is:

$$\mathbf{y} = \begin{bmatrix} \Omega_m + n_o \\ z_m + n_p \end{bmatrix}, \quad (2)$$

where Ω_m is the optic flow measurements from optic flow sensor, z_m is the measurement from the pressure sensor, and n_o and n_p are the noise terms for the two sensors. We assume noise terms are zero-mean Gaussian white noise, a standard assumption in sensor noise modeling to simplify the analysis. The measurement model for the optic flow in the x direction, as measured by the optic flow camera is a nonlinear function of state [6]:

$$\Omega_m = \omega_m - \frac{v_x}{z}, \quad (3)$$

where ω_m is the angular velocity measurement from gyroscope. We can see the optic flow measurement depends on z . We can take the Jacobian linearization at a desired altitude z_d :

$$\Omega_m(z) = \Omega_m(z_d) + O(z) = \omega_m - \frac{v_x}{z_d} + O(z). \quad (4)$$

With this linearization, our measurement model can be cast into the traditional Kalman Filter model, $\mathbf{y} = C\mathbf{q} + D\mathbf{u} + \mathbf{n}$, where

$$C = \begin{bmatrix} 0 & -\frac{1}{z_d} & 0 \\ 0 & 0 & 1 \end{bmatrix}, \quad D = \begin{bmatrix} 1 \\ 0 \end{bmatrix}. \quad (5)$$

The observability matrix $[C; CA]$ is full rank, meaning that a Kalman Filter will be able to estimate the system’s state using the measurements given in Eq. (5).

The Kalman Filter observer estimates $\hat{\mathbf{q}}$ by numerically integrating the system

$$\dot{\hat{\mathbf{q}}} = A\hat{\mathbf{q}} + B\mathbf{u} + K(\mathbf{y} - C\hat{\mathbf{q}} - D\mathbf{u}), \quad (6)$$

where K is the Kalman gain.

We used a gradient descent algorithm to minimize the RMSE between the TinySense state estimates and the mocap ground-truth to tune the process noise covariance matrix Qn and sensor noise covariance matrix Rn :

$$Qn = \text{diag}(0.14^2, 0.093^2, 0.08^2), \quad Rn = \text{diag}(1.06^2, 0.2^2).$$

For the process noise (disturbance) matrix G , we assumed that the noise enters the system as white noise disturbance adding to the derivatives of the three states θ , v_x , and z . Based on these, the Kalman gain K was computed using the `lqe` command in `python-control` [34].

$$G = \begin{bmatrix} 0.72 & 0 & 0 \\ 0 & 0.10 & 0 \\ 0 & 0 & 20.00 \end{bmatrix}, \quad K = \begin{bmatrix} 0.00204 & 0 \\ 0.48452 & 0 \\ 0 & 1.81818 \end{bmatrix}.$$

We implemented the Kalman Filter offline in Python by iteratively computing the state estimates $\hat{\mathbf{q}}_{i+1}$ according to $\hat{\mathbf{q}}_{i+1} = \hat{\mathbf{q}}_i + \dot{\hat{\mathbf{q}}}_i \cdot dt$.

V. EXPERIMENTS

A. Robot platform

We performed experiments using Crazyflie 2.0, a palm-sized quadrotor by Bitcraze (Sweden), in wind-free conditions in an indoor environment. In addition to its built-in gyroscope, the Crazyflie was equipped with the Flow deck v2 consisting of a downward-facing optic flow sensor and a laser rangefinder; it uses an Extended Kalman Filter to estimate its state in flight [35].

B. Motion capture system

To provide a ground-truth comparison for the sensors, we used a twelve-camera OptiTrack Flex 13 motion capture arena. The Crazyflie drone was fitted with four retro-reflective motion capture markers and its position and orientation were recorded at 120 Hz. Velocity was estimated by taking the numerical derivative of the position data in post-processing.

C. Experiment

We connected our sensor suite to an NRF52840 Express (Adafruit), a board which supports data transmission through UART and 2.4GHz Bluetooth Low Energy compatibility. We mounted the board as close to the geometrical center of the Crazyflie as possible to maintain a reasonable center of mass and minimize vibration interference to the IMU from the

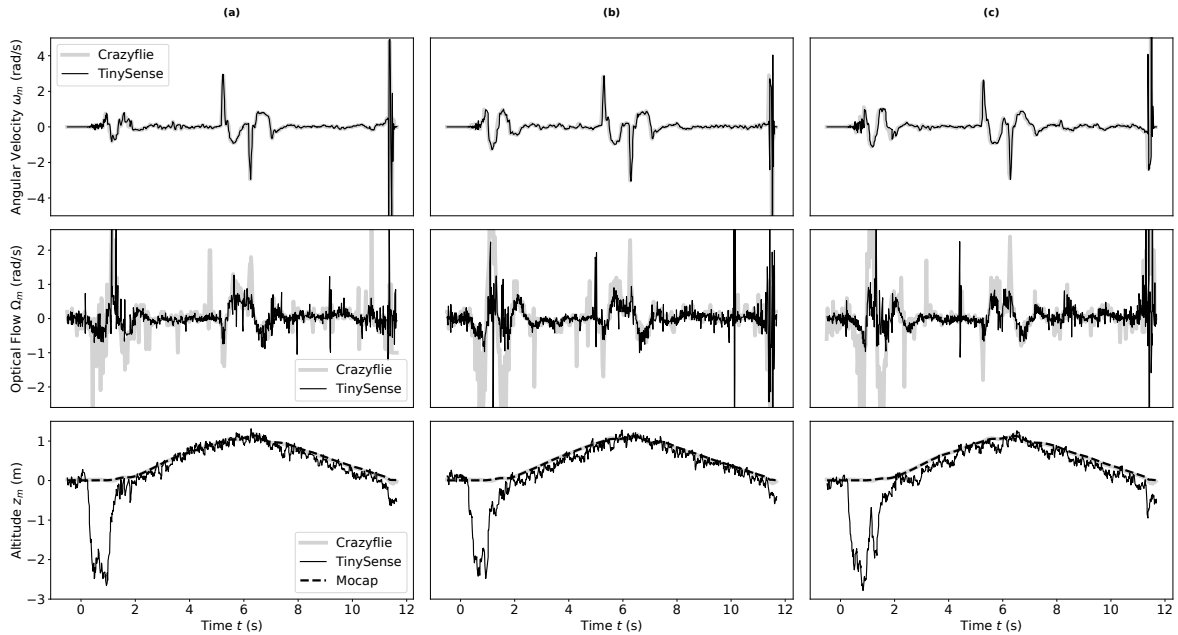


Fig. 4: Sensor measurements from the onboard gyroscope, optic flow sensor, and pressure sensor of TinySense are compared with those from the Crazyflie for three different flight experiments (a), (b), and (c). In the altitude plots, altitude is measured by the Crazyflie’s laser rangefinder, while the TinySense uses a pressure sensor; mocap data is also included for comparison.

propellers. Power was supplied from the Crazyflie’s 250mAh Lithium Polymer (LiPo) battery.

Each trial consisted of commanding the robot to rise to an altitude of 1 m, translate forward 1 m at 1 m/s, and then descend back to the ground. We ran this experiment three times. We collected measurements from the TinySense’s sensors on a laptop as they were transmitted over Bluetooth at 100 Hz as binary data. Simultaneously, a second computer captured motion capture data at 120 Hz and used a Python-based script to capture sensor measurements and state estimates transmitted from the Crazyflie over Bluetooth at its maximum rate of 30 Hz. Each receiving device independently recorded a UTC timestamp, which was used to synchronize the data. The sensor measurements from the TinySense compared with the Crazyflie, and the motion capture (mocap) system’s measurement for altitude are shown in Fig. 4.

D. Computational Load

We estimated the power consumption of the optic flow algorithm from the number of cycles in a single run. We focus on only estimating three types of operations conducted on the ARM Cortex-M4 based microcontroller: single-cycle operations (addition, subtraction, multiplication, and memory read/write); integer divisions, which require 12 cycles at most; and floating-point divisions, which require 14 cycles. These results are summarized in Table II. Given that in our current system, all sensors update at a rate of 100 Hz, we gather that the total number of cycles per second is ~ 24.98 Mhz. Operating on the nRF52840 chip with an efficiency of $52 \mu\text{A/Mhz}$ and a battery-powered voltage of 4.2V, we estimate the power use of the optic flow algorithm to be

$\sim 5.45\text{mW}$.

E. Results and Discussions

Fig. 5 compares our sensor suite’s state estimate to that of the Crazyflie’s built-in estimator, and states derived from the mocap system, considered to be ground truth. For the state estimator, time $t = 0$ corresponds to when the gyroscope reading becomes significantly different from zero, indicating liftoff. It can be observed in Fig. 4 that a pressure increase occurs when the propellers first turn on, which can be observed as a drop in measured altitude. To mitigate unwanted effects of this in the Kalman Filter, we ignored (set to zero) altitude measurements z_m during the first 1.8s after liftoff. Nevertheless, once it is in the air, the altitude measurement matches quite closely with the laser rangefinder on the Crazyflie, though with slightly more noise.

Our system’s estimate compares well with those of the Crazyflie’s, despite receiving gyroscope readings at a much lower rate (100 Hz) compared to 1000 Hz on the Crazyflie[35]. The RMSE is approximately equal for pitch angle (Table III). We observe that there are occasionally large errors in translational velocity v_x . These appear to occur after sudden changes in attitude that occur around $t = 5$ s and $t = 6$ s, during which the angular velocity momentarily exceeds 3 rad/s (Fig. 4). We note that at these moments, our TinySense optic flow sensor’s readings are consistently lower than those of the Crazyflie. Lucas-Kanade cannot detect motion accurately if the displacement between frames is greater than a half pixel between image frames. The maximum allowable angular velocity is given by $\Omega = 0.5\alpha F = (0.5)(0.027)(100) = 1.4$ rad/s, where α is the

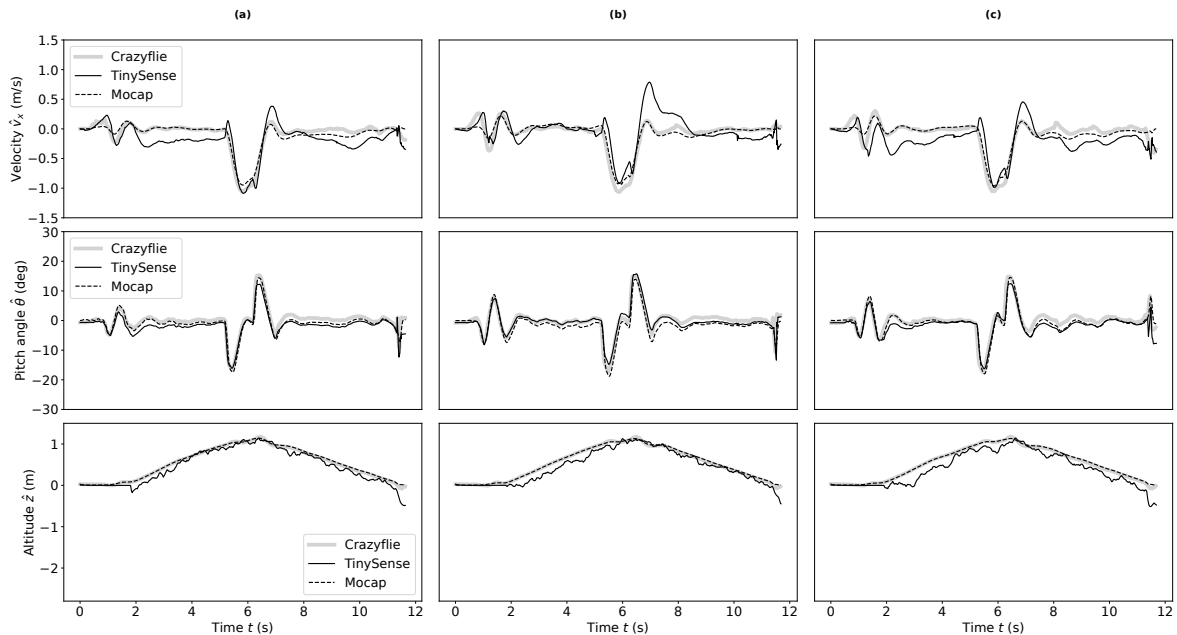


Fig. 5: State estimates from TinySense after Kalman filtering, Crazyflie estimates, and mocap estimates are compared. We conducted three flight experiments (a), (b), and (c), with the Kalman filter estimates starting at time zero. Note that we ignore the pressure sensor measurements in the first 1.8s because of the pressure change near the surface.

TABLE II: Estimation of Optic Flow Algorithm Power Use

Update Frequency (Hz)	Occurrences/Update	Step Name	Single-cycle Operations	Int Division Operations	Floating-point Division Operations	Total Cycles/Update	Total Cycles/Second	Power Use
100	1	Skip frame	8493	0	8	249781	24.9781 Mhz	~5.4552mW
	12	LK OF	18434	128	2			
	1	Copy data	1200	0	0			

TABLE III: Root Mean Squared Error (RMSE) of estimates relative to mocap system

	velocity v_x (m/s)	pitch angle θ (deg)	altitude z (m)
Crazyflie	0.075 ± 0.009	1.619 ± 0.267	0.021 ± 0.001
TinySense	0.186 ± 0.015	1.573 ± 0.166	0.139 ± 0.026

angular increment between neighboring pixels (Section II-A) and F is the frame rate in Hz. So the expected optic flow is faster than can be detected. This could be mitigated by a faster frame rate or a larger angular displacement between pixels.

VI. CONCLUSION

In the present study, we introduce a new sensor suite with dramatically reduced mass, and associated optic flow and state estimation software that is compatible with the computational constraints of an onboard microcontroller small enough to fly aboard flying insect robots (FIRs) weighing less than a gram. Our proposed avionics suite diverges in two important ways compared to that of the 28 g Crazyflie helicopter, the lightest vehicle yet to perform controlled hovering, and previous work [15]. First, it replaces a power-hungry laser rangefinder with a much more efficient (and slightly less ideal) and lighter pressure sensor. Second,

we replaced an off-the shelf optic flow sensor, which is available only in relatively heavy packages, with a custom camera with a global shutter and a custom-written Lucas-Kanade-based optic flow algorithm running onboard a 10 mg microcontroller small enough to fly onboard an FIR (estimated compute power usage is about 5 mW). Our system uses a Kalman Filter to estimate pitch angle, translational velocity, and altitude. Remarkably, the cumulative weight of this sensor suite is only 78.4 mg, rather less than the 187 mg of previous work [15]. Incorporating a microcontroller to this configuration, the overall system remains well within the anticipated 252 mg payload limit of the 143 mg robotic platform reported in [18]. Our system demonstrates average RMSE values of 0.186 m/s for velocity, 1.573 degrees for pitch angle, and 0.139 meters for altitude when compared to the motion capture system. In comparison, the Crazyflie platform achieves RMSE values of 0.075 m/s, 1.619 degrees, and 0.021 meters for the same states during similar flight maneuvers. This shows that our system performs closely to the state-of-the-art Crazyflie in these scenarios. In future work, we aim to integrate TinySense with insect-scale robots to perform more advanced tasks, such as confined-space navigation [36].

REFERENCES

- [1] K. Y. Ma, P. Chirarattananon, S. B. Fuller, and R. J. Wood, "Controlled flight of a biologically inspired, insect-scale robot," *Science*, vol. 340, no. 6132, pp. 603–607, 2013.
- [2] S. Kim, Y.-H. Hsiao, Y. Chen, J. Mao, and Y. Chen, "Firefly: An insect-scale aerial robot powered by electroluminescent soft artificial muscles," *IEEE Robotics and Automation Letters*, vol. 7, no. 3, pp. 6950–6957, 2022.
- [3] J. M. James, V. Iyer, Y. M. Chukewad, S. Gollakota, and S. B. Fuller, "Lift-off of a 190 mg laser-powered aerial vehicle: The lightest wireless robot to fly," in *Robotics and Automation (ICRA), IEEE Int. Conf.*, 2018, pp. 1–8.
- [4] N. T. Jafferis, E. F. Helbling, M. Karpelson, and R. J. Wood, "Untethered flight of an insect-sized flapping-wing microscale aerial vehicle," *Nature*, vol. 570, pp. 491–495, 2019.
- [5] T. Ozaki, N. Ohta, T. Jimbo, and K. Hamaguchi, "A wireless radiofrequency-powered insect-scale flapping-wing aerial vehicle," *Nature Electronics*, vol. 4, no. 11, pp. 845–852, 2021.
- [6] S. Fuller, Z. Yu, and Y. P. Talwekar, "A gyroscope-free visual-inertial flight control and wind sensing system for 10-mg robots," *Science Robotics*, vol. 7, no. 72, p. eabq8184, 2022.
- [7] W. S. N. Trimmer, "Microbots and micromechanical systems," *Sensors and Actuators*, vol. 19, pp. 267–287, 1989.
- [8] G. Caprari, T. Estier, and R. Siegwart, "Fascination of down scaling—alice the sugar cube robot," *Journal of micromechatronics*, vol. 1, no. 3, pp. 177–189, 2001.
- [9] J. J. Abbott, Z. Nagy, F. Beyeler, and B. J. Nelson, "Robotics in the small, part i: microbotics," *IEEE Robotics & Automation Magazine*, vol. 14, no. 2, pp. 92–103, 2007.
- [10] I. Paprotny and S. Bergbreiter, "Small-scale robotics: An introduction," in *workshop at the IEEE International Conference on Robotics and Automation*. Springer, 2013, pp. 1–15.
- [11] D. Floreano and R. J. Wood, "Science, technology and the future of small autonomous drones," *Nature*, vol. 521, no. 7553, pp. 460–466, 2015.
- [12] H. D. Escobar-Alvarez, N. Johnson, T. Hebble, K. Klingebiel, S. A. P. Quintero, J. Regenstein, and N. A. Browning, "R-advance: Rapid adaptive prediction for vision-based autonomous navigation, control, and evasion," *Journal of Field Robotics*, vol. 35, no. 1, pp. 91–100, 2018. [Online]. Available: <http://dx.doi.org/10.1002/rob.21744>
- [13] D. Palossi, A. Loquercio, F. Conti, E. Flamand, D. Scaramuzza, and L. Benini, "A 64mw dnn-based visual navigation engine for autonomous nano-drones," *IEEE Internet of Things Journal*, 2019.
- [14] M. B. Kjergaard, H. Blunck, T. Godsk, T. Toftkjær, D. L. Christensen, and K. Grønbæk, "Indoor positioning using gps revisited," in *Pervasive Computing: 8th International Conference, Pervasive 2010, Helsinki, Finland, May 17-20, 2010. Proceedings 8*. Springer, 2010, pp. 38–56.
- [15] Y. P. Talwekar, A. Adie, V. Iyer, and S. B. Fuller, "Towards sensor autonomy in sub-gram flying insect robots: A lightweight and power-efficient avionics system," in *2022 International Conference on Robotics and Automation (ICRA)*. IEEE, 2022, pp. 9675–9681.
- [16] S. B. Fuller, M. Karpelson, A. Censi, K. Y. Ma, and R. J. Wood, "Controlling free flight of a robotic fly using an onboard vision sensor inspired by insect ocelli," *Journal of The Royal Society Interface*, vol. 11, no. 97, p. 20140281, 2014.
- [17] N. O. Pérez-Arancibia, K. Y. Ma, K. C. Galloway, J. D. Greenberg, and R. J. Wood, "First controlled vertical flight of a biologically inspired microrobot," *Bioinspiration and Biomimetics*, vol. 6, no. 3, p. 036009, Sep 2011. [Online]. Available: <http://dx.doi.org/10.1088/1748-3182/6/3/036009>
- [18] D. S. Drew and K. S. Pister, "First takeoff of a flying microrobot with no moving parts," in *Manipulation, Automation and Robotics at Small Scales (MARSS), 2017 International Conference on*, 2017, pp. 1–5.
- [19] M. Karásek, F. T. Muijres, C. De Wagter, B. D. Remes, and G. C. de Croon, "A tailless aerial robotic flapper reveals that flies use torque coupling in rapid banked turns," *Science*, vol. 361, no. 6407, pp. 1089–1094, 2018.
- [20] S. B. Fuller, "Four wings: An insect-sized aerial robot with steering ability and payload capacity for autonomy," *IEEE Robotics and Automation Letters*, vol. 4, no. 2, pp. 570–577, 2019.
- [21] S. B. Fuller, Z. E. Teoh, P. Chirarattananon, N. O. Pérez-Arancibia, J. Greenberg, and R. J. Wood, "Stabilizing air dampers for hovering aerial robotics: design, insect-scale flight tests, and scaling," *Autonomous Robots*, February 2017. [Online]. Available: <http://dx.doi.org/10.1007/s10514-017-9623-3>
- [22] H. K. Hari Prasad, R. S. Vaddi, Y. M. Chukewad, E. Dedic, I. Novoselov, and S. B. Fuller, "A laser-microfabricated electrohydrodynamic thruster for centimeter-scale aerial robots," *PLoS one*, vol. 15, no. 4, p. e0231362, 2020.
- [23] Z. E. Teoh, S. B. Fuller, P. C. Chirarattananon, N. O. Pérez-Arancibia, J. D. Greenberg, and R. J. Wood, "A hovering flapping-wing micro-robot with altitude control and passive upright stability," in *Intelligent Robots and Systems (IROS), 2012 IEEE/RSJ Int. Conf.*, Vilamoura, Algarve, Portugal, 7–12 October 2012, pp. 3209–3216.
- [24] S. B. Fuller, M. Karpelson, A. Censi, K. Y. Ma, and R. J. Wood, "Controlling free flight of a robotic fly using an onboard vision sensor inspired by insect ocelli," *J. Royal Society Interface*, vol. 11, no. 97, August 2014. [Online]. Available: <http://rsif.royalsocietypublishing.org/content/11/97/20140281.abstract>
- [25] Y. M. Chukewad, J. M. James, A. Singh, and S. B. Fuller, "Robofly: An insect-sized robot with simplified fabrication that is capable of flight, ground, and water surface locomotion," *IEEE Transactions on Robotics*, 2021, (in press).
- [26] R. J. Wood, "The first takeoff of a biologically inspired at-scale robotic insect," *IEEE Trans. Robotics*, vol. 24, no. 2, pp. 341–347, 2008.
- [27] A. Beyeler, "Vision-based control of near-obstacle flight," Ph.D. dissertation, ÉCOLE POLYTECHNIQUE FÉDÉRALE DE LAUSANNE, 2009.
- [28] G. K. Taylor and H. G. Krapp, "Sensory systems and flight stability: What do insects measure and why?" in *Insect Mechanics and Control*, ser. Advances in Insect Physiology, J. Casas and S. Simpson, Eds. New York: Academic Press, 2007, vol. 34, pp. 231–316. [Online]. Available: <http://www.sciencedirect.com/science/article/pii/S0065280607340058>
- [29] J. J. Koenderink and A. J. van Doorn, "Facts on optic flow," *Biological Cybernetics*, vol. 56, pp. 247–254, 1987.
- [30] B. D. Lucas, T. Kanade, et al., "An iterative image registration technique with an application to stereo vision." in *IJCAI*, vol. 81, 1981, pp. 674–679.
- [31] B. K. P. Horn and B. G. Schunck, "Determining optical flow," *Artificial Intelligence*, vol. 17, pp. 185–203, 1981.
- [32] R. Hartley and A. Zisserman, *Multiple view geometry in computer vision*. Cambridge university press, 2003.
- [33] C. D. Wagter, S. Tijmons, B. Remes, and G. de Croon, "Autonomous flight of a 20-gram flapping wing mav with a 4-gram onboard stereo vision system," in *Robotics and Automation (ICRA), 2014 IEEE Int. Conf.* Hong Kong, China: IEEE, 2–5 June 2014.
- [34] S. Fuller, B. Greiner, J. Moore, R. Murray, R. van Paassen, and R. Yorke, "The python control systems library (python-control)," in *2021 60th IEEE Conference on Decision and Control (CDC)*. IEEE, 2021, pp. 4875–4881.
- [35] M. W. Mueller, M. Hamer, and R. D'Andrea, "Fusing ultra-wideband range measurements with accelerometers and rate gyroscopes for quadcopter state estimation," in *2015 IEEE International Conference on Robotics and Automation (ICRA)*, May 2015, pp. 1730–1736.
- [36] Z. Yu, G. Zardini, A. Censi, and S. Fuller, "Visual confined-space navigation using an efficient learned bilinear optic flow approximation for insect-scale robots," in *2022 IEEE/RSJ International Conference on Intelligent Robots and Systems (IROS)*. IEEE, 2022, pp. 4250–4256.